Mon. Not. R. Astron. Soc. **000**, 1–9 (0000) Printed 5 February 2008 (MN LATEX style file v2.2)

A dynamo model for axisymmetric and non-axisymmetric solar magnetic fields

J. Jiang⋆ and J. X. Wang⋆
National Astronomical Observatories, Chinese Academy of Sciences, Beijing 100012, China

arXiv:astro-ph/0702508v1 20 Feb 2007

Accepted 0000 xxxx 00. Received 0000 xxxx 00; in original form 0000 xxxx 00

ABSTRACT
Increasing observations are becoming available about a relatively weak, but persistent, non-axisymmetric magnetic field co-existing with the dominant axisymmetric field on the Sun. It indicates that the non-axisymmetric magnetic field plays an important role in the origin of solar activity. A linear non-axisymmetric $\alpha^2-\Omega$ dynamo model is set up to discuss the characteristics of the axisymmetric ($m=0$) and the first non-axisymmetric ($m=1$) modes and to provide further the theoretical bases to explain the 'active longitude', 'flip-flop' and other non-axisymmetric phenomena. The model consists of a updated solar internal differential rotation, a turbulent diffusivity varied with depth and an α-effect working at the tachocline in rotating spherical systems. The difference between the $\alpha^2-\Omega$ and the $\alpha-\Omega$ models and the conditions to favor the non-axisymmetric modes with the solar-like parameters are also presented.

Key words: magnetic fields – MHD – Sun: activity – Sun: magnetic fields.

1 INTRODUCTION

The distribution of magnetic field emerging on the solar surface carries clues to the mechanism of the field generation. One striking feature of this distribution is clustering of active regions which is commonly called 'active longitude' (Bai 1987; Benevolenskaya et al. 1999; De Toma, White & Harvey 2000). Signatures of possible longitudinal inhomogeneities have also been reported in the distributions of solar wind and interplanetary magnetic field (Neugebauer et al. 2000). Furthermore, 'flip-flop' phenomenon, i.e. the two persistent active longitudes separated by 180°, has also been identified on the Sun (Berdyugina & Usoskin 2003). These observations indicate the involvement of large-scale non-axisymmetric magnetic field in the formation and evolution of the dominant axisymmetric solar activities. Hence, it is valuable to set up the non-axisymmetric dynamo model to explain these non-axisymmetric solar magnetic fields.

The pioneer works on the theoretical investigations of the non-axisymmetric activities can be classed mainly as two kinds. One is that the generation sources are non-axisymmetric, and the non-axisymmetric magnetic field is produced accordingly. For example, Bigazzi & Ruzmaikin (2004) and Moss et al. (2002) adopted the non-axisymmetric distribution of α-effect. The other is based on the axisymmetric sources of generation but to excite the non-axisymmetric field. The numerical results of Chan et al. (2004) supported this possibility.

Earlier studies (Stix 1971; Ivanova & Ruzmaikin 1985) concerning the linear non-axisymmetric solar dynamo with decoupled axisymmetric and non-axisymmetric modes have been taken. But these earlier studies could not include the correct distribution of solar differential rotation, which was unknown at that time. Recently, there are some works on the non-linear non-axisymmetric dynamo models. Moss (1999) obtained stable solutions which possessed a small non-axisymmetric field component co-existing with a dominant axisymmetric part with the updated solar rotation profile. Bigazzi & Ruzmaikin (2004) studied the generation of non-axisymmetric fields and their coupling with the axisymmetric solar magnetic field. Bassom et al. (2005) used an asymptotic WKBJ method to investigate a linear $\alpha^2-\Omega$ model with the aim to isolate the basic physical effects leading to the preferable excitation of non-axisymmetric solar and stellar magnetic structure. However, are there possibilities to work out a linear non-axisymmetric solar dynamo with the updated generation sources to relate with the non-axisymmetric phenomena? What are the differences, such as configuration and cycle and so on, between the axisymmetric and non-axisymmetric modes? When will the non-axisymmetric mode be preferred? These are the main objectives of the paper.

With the axisymmetric sources of generation, we develop a new high-precision non-axisymmetric code based on the spectral method and begin with the linear non-axisymmetric mean field dynamo equations. The axisym-

⋆ E-mail: jiangjie@ourstar.bao.ac.cn (JJ); wangjx@bao.ac.cn

metric mode $m = 0$ and the first non-axisymmetric mode $m = 1$ are discussed, respectively, in Sec.5 and Sec.6. We will show the difference between the $\alpha^2 - \Omega$ and the $\alpha - \Omega$ models in Sec.3. In Sec. 4, the condition to excite the dominant axisymmetric mode and the condition to favor the non-axisymmetric mode will be discussed.

2 MATHEMATIC FORMULATIONS

2.1 The basic equations

The starting point of our model is the mean field dynamo equation, governing the evolution of the large-scale magnetic field $\boldsymbol{B}$ in response to the flow field $\boldsymbol{U}$, the α-effect and the magnetic diffusivity η:

$$\frac{\partial \boldsymbol{B}}{\partial t} = \nabla \times [\boldsymbol{U} \times \boldsymbol{B} + \alpha \boldsymbol{B} - \eta \nabla \times \boldsymbol{B}]. \quad (1)$$

Since the turbulent diffusivity is much larger than the molecular diffusivity, we ignore the molecular diffusivity in η. For the flow field, only the (differential) rotation Ω is considered for simplicity. Since the magnetic field is divergence-free, we expand $\boldsymbol{B}$ in term of two scalar functions h and g which represent the poloidal and toroidal potentials, respectively, in the spherical polar coordinates (r, θ, ϕ) as Chandrasekhar (1961) and Moffatt (1978).

$$\boldsymbol{B} = \nabla \times \nabla \times \boldsymbol{r} h(r, \theta, \phi, t) + \nabla \times \boldsymbol{r} g(r, \theta, \phi, t). \quad (2)$$

When $\alpha = \alpha(r, \theta)$, $\Omega = \Omega(r, \theta)$, $\eta = \eta(r)$, substituting equation(2) in equation (1), the governing equation reduces to:

$$\partial_t L^2 h = R_\alpha V_\alpha^g + \eta \nabla^2 L^2 h + R_\Omega V_{\Omega N}^h + R_\alpha V_{\alpha N}^h, \quad (3)$$

$$\partial_t L^2 g = R_\alpha V_\alpha^h + R_\Omega V_\Omega^h + R_\Omega V_{\Omega N}^g + R_\alpha V_{\alpha N}^g + \eta \nabla^2 L^2 g + \frac{\partial \eta}{\partial r}\frac{\partial}{\partial r} L^2 g + \frac{1}{r}\frac{\partial \eta}{\partial r} L^2 g, \quad (4)$$

where

$$L^2 = -\frac{1}{\sin\theta}\frac{\partial}{\partial \theta}(\sin\theta \frac{\partial}{\partial \theta}) - \frac{1}{\sin^2\theta}, \nabla^2 = \frac{1}{r}\frac{\partial}{\partial r} r^2 \frac{\partial}{\partial r} - \frac{1}{r^2} L^2.$$

$V_{\Omega N}$ and $V_{\alpha N}$ are the terms which have the azimuthal component $\partial/\partial\phi$ and V_Ω, $V_\alpha, V_{\Omega N}$ and $V_{\alpha N}$ can be obtained from (see Appendix):

$$\boldsymbol{r} \cdot \nabla \times (\alpha \boldsymbol{B}) = V_\alpha^g + V_{\alpha N}^h, \quad (5)$$

$$\boldsymbol{r} \cdot \nabla \times (\boldsymbol{U} \times \boldsymbol{B}) = V_{\Omega N}^h, \quad (6)$$

$$\boldsymbol{r} \cdot \nabla \times [\nabla \times (\alpha \boldsymbol{B})] = V_\alpha^h + V_{\alpha N}^g, \quad (7)$$

$$\boldsymbol{r} \cdot \nabla \times [\nabla \times (\boldsymbol{U} \times \boldsymbol{B})] = V_\Omega^h + V_{\Omega N}^g. \quad (8)$$

The equations (3) and (4) have been cast in non-dimensional form by expressing all lengths in units of solar radius $R_\odot$ and time in units of the magnetic diffusion time $R_\odot^2/\eta_o$. This has led to the appearance of two dimensionless numbers:

$$R_\alpha = \frac{\alpha_o R_\odot}{\eta_o}, \quad (9)$$

$$R_\Omega = \frac{\Omega_o R_\odot^2}{\eta_o}, \quad (10)$$

where α_o and η_o are reference values for the α-effect and the diffusivity in the convective zone (CZ), respectively. And Ω_o is the characteristic value of the differential rotation. The quantities R_α and R_Ω are dynamo numbers measuring the relative importance of inductive versus diffusive effects. More discussion about R_Ω will be given in Subsection 2.2.

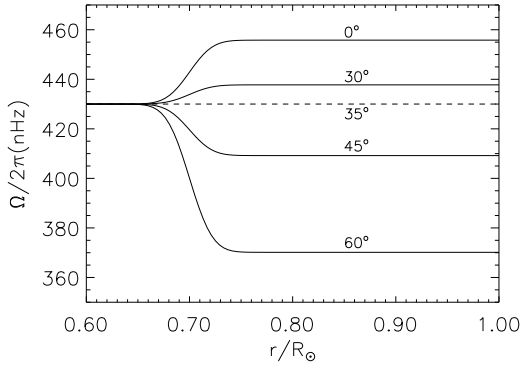

Figure 1. Radial distributions of solar rotation at different latitudes. There are strong radial shear in the high latitude of the tachocline. At 35° latitude, the shear is very weak (dashed line).

2.2 Internal rotation $\Omega(r, \theta)$

Based on the helioseismic inversion (Schou et al. 1998; Charbonneau et al. 1999), there are two strong radial shear regions inside of the Sun. One is in the tachocline and the other locates in sub-photospheric layer. For the sake of simplicity on computational solutions, We neglect the shear at the sub-surface and regard that the dynamo works in the tachocline. The following expression for the solar interior rotation is adopted.

$$\Omega(r, \theta) = \Omega_c + \frac{1}{2}[1 + erf(2\frac{r - r_c}{d})](\Omega_s(\theta) - \Omega_c), \quad (11)$$

where $\Omega_s(\theta) = \Omega_{EQ} + a_2 \cos^2\theta + a_4 \cos^4\theta$ is the surface latitudinal rotation and θ is co-latitude. The parametric values are set as $r_c = 0.7 R_\odot$, $d = 0.05 R_\odot$, $\Omega_c/2\pi = 430.0$ nHz, $\Omega_{EQ}/2\pi = 455.8$ nHz, $a_2/2\pi = -51.2$ nHz, $a_4/2\pi = -84.0$ nHz. Fig. 1 shows the radial distribution of $\Omega(r, \theta)$ at different latitudes. It reveals that Ω depends weakly on depth in bulk of CZ. But in the tachocline, the rotation rate changes from almost uniform in the radiative interior to depth dependent in the CZ. Within the tachocline, rotation increases with distance from the core at low latitudes, while it decreases at high latitudes. At intermediate latitudes (near 35°, dashed line in Fig. 1) rotation is almost independent on the depth.

Furthermore, we base our model on the rotating spherical systems with the rotation velocity Ω_c of the inner core. Thus the differential rotation in the rotating frame Ω_c is

$$\Omega'(r, \theta) = \frac{1}{2}[1 + erf(2\frac{r - r_c}{d})](2\pi \times 25.8) \times (1. - 1.98\cos^2\theta - 3.26\cos^4\theta) \text{ (nHz)}. \quad (12)$$

The differential rotation of the surface at the equator is $(2\pi \times 25.8)$ nHz and we regard it as the characteristic value of the differential rotation Ω_o in Eq. (10). Hence, the value of R_Ω is adopted as $\frac{8 \times 10^{10}\ \mathrm{m^2 s^{-1}}}{\eta_o}$, which is only decided by the reference value of the diffusivity η_o.

2.3 The diffusivity profile $\eta(r)$

We use the analytical expression of Dikpati & Charbonneau (1999) for the diffusivity profile as

$$\eta(r) = \eta_c + \frac{\eta_o}{2}[1 + erf(2\frac{r - r_c}{d})], \quad (13)$$

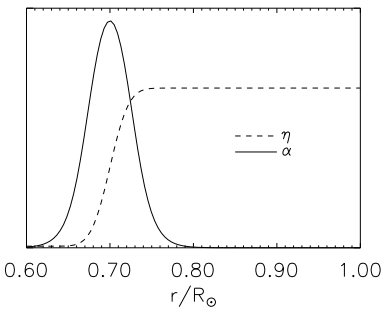

Figure 2. Radial distributions of the α-effect (solid line) which mainly concentrate in the tachocline and the magnetic diffusivity η (dashed line). Values of y-axis are not scaled.

whose distribution can be seen in Fig. 2 (dashed line). The diffusivity η_o in CZ, is dominated by the turbulence. In the stably stratified core, the diffusivity η_c is much lower because of the much less turbulence. In what follows we take η_c/η_o=0.01. The transition from high to low diffusivity occurs near the tachocline, which is coincident with the rotational shear layer. Here, η_o is far less definite and is widely known to fall in the range from 2×10^{10} cm^{2}s^{-1} to 2×10^{12} cm^{2}s^{-1}.

2.4 The α-effect $\alpha(r,\theta)$

The α-effect cannot yet be determined from observations. The dominated physical mechanisms responsible for it can be categorized as the following three types. (1) It works at the surface produced by the decaying of active regions (Babcock 1961; Leighton 1969). (2) It is directly related to turbulent convective motions (Parker 1955). It exists throughout the whole CZ and changes sign near the bottom of the CZ (Krivodubskii 1998; Kuzanyan et al. 2003). (3) It works at the tachocline induced by the hydrodynamical shear instabilities (Dikpati et al. 2001) or MHD instabilities (Thelen 2000). It is possible that all of them work simultaneously inside of the Sun. Here, we only consider the α-effect concentrating in the tachocline with the following expression

$$\alpha(r,\theta) = \alpha_o \frac{1}{2}[1+erf(2\frac{r-r_1}{d})] \frac{1}{2}[1-erf(2\frac{r-r_2}{d})]\cos\theta, \quad (14)$$

where $r_1=0.675R_\odot$, $r_2=0.725R_\odot$. The solid line in Fig. 2 shows the variation of $\alpha(r,\theta)$ with r, which is mainly concentrated in the tachocline. The common angular dependence $\cos\theta$ is adopted, the simplest guaranteeing antisymmetry across the equator. Moreover, we do not consider the α-quenching since only the linear solutions are sought.

2.5 The numerical scheme

Since the governing equations (3) and (4) are two coupled, linear homogeneous equations in h and g, with the given boundary conditions, we can look for their eigensolutions with the form

$$[h(r,\theta,\phi,t),g(r,\theta,\phi,t)]=[h(r,\theta,\phi),g(r,\theta,\phi)]\mathrm{e}^{st}, \quad (15)$$

where s is the eigenvalue and can be written as $s=\sigma+i\omega$. Only the solution that neither grows nor decays ($\sigma\simeq0$), i.e. the onset of dynamo actions is considered. The corresponding R_α is the critical R_α. The solution with the lowest dynamo number is the easiest to excite and is the most stable one. In what immediately follows, we solve the dynamo equations numerically using spectral (Chebyshev-τ) method (see Jiang & Wang 2006 for detail).

Different azimuthal modes m are decoupled in linear theory. For given m, we expand h and g at the onset of the dynamo action in terms of Chebyshev polynomial $T_n(r)$ and surface harmonics $P_l^m\mathrm{e}^{\mathrm{i}m\phi}$ in the meridional circular sector $r\in[0.6,1.0]$, $\theta\in[0.0,\pi]$ as follows:

$$h=\sum_{n=0}^{N}\sum_{l=m}^{L}c_{n,l}^h T_n(ar-b)P_l^m(\cos\theta)\mathrm{e}^{\mathrm{i}m\phi}, \quad (16)$$

$$g=\sum_{n=0}^{N}\sum_{l=m}^{L}c_{n,l}^g T_n(ar-b)P_l^m(\cos\theta)\mathrm{e}^{\mathrm{i}m\phi}, \quad (17)$$

where $ar-b\in[-1,+1]$. Here, N and L are the truncations needed to get convergence. It varies with different dynamo number and different Ω, η, α profiles. $c_{n,l}^h$ and $c_{n,l}^g$ are eigenvectors.

At two interface $r=r_o=1.0$ and $r=r_i=0.6$, both magnetic field and the tangential electric field must be continuous. The exterior $r>1.0$ is a vacuum and eigensolutions are matched to a potential field. The radiative core is assumed to behave as a perfect conductor. We may obtain (see Schubert & Zhang 2001 for detail):

$$\text{at } \mathrm{r}=\mathrm{r_i}=0.6,\quad \sum_{\mathrm{n}}\sum_{\mathrm{l}}\mathrm{c}_{\mathrm{n,l}}^{\mathrm{h}}(-1)^{\mathrm{n}}\mathrm{P}_{\mathrm{l}}^{\mathrm{m}}(\cos\theta) = 0, \quad (18)$$

$$\sum_{n}\sum_{l}c_{n,l}^h[a(-1)^{n+1}n^2r_i+(-1)^n]P_l^m(\cos\theta) = 0, \quad (19)$$

$$\text{at } \mathrm{r}=\mathrm{r_o}=1.0,\quad \sum_{\mathrm{n}}\sum_{\mathrm{l}}\mathrm{c}_{\mathrm{n,l}}^{\mathrm{g}}\mathrm{P}_{\mathrm{l}}^{\mathrm{m}}(\cos\theta) = 0, \quad (20)$$

$$\sum_{n}\sum_{l}c_{n,l}^h[an^2r_o+(1+l)]P_l^m(\cos\theta) = 0. \quad (21)$$

As pointed out by Ivanova & Ruzmaikin (1985), the system of Eqs. (3) and (4) may be decomposed into two subsystems, i.e. odd or even parity with respect to the equatorial plane. We denote them by A and S. With the parameters adopted in our model, both odd and even parity solutions have nearly the same dynamo number for given mode m. Therefore, we cannot decide which kind of symmetric solution is excited easier. However, according to the observations and theoretical computations (Moss 2004; Fluri & Berdyugina 2004), the dipolar mode ($A0$) for axisymmetric field and the perpendicular dipolar mode ($S1$) for non-axisymmetric field are definitely identified on the Sun although there are some possibilities for some other non-axisymmetric modes exist on the Sun (De Toma, White & Harvey 2000; Song & Wang 2005). Hence we will only choose the two modes $A0$ and $S1$ as the representatives of axisymmetric and non-axisymmetric modes, respectively and investigate $A0$ and $S1$ in detail below. We firstly discuss the difference between the $\alpha^2-\Omega$

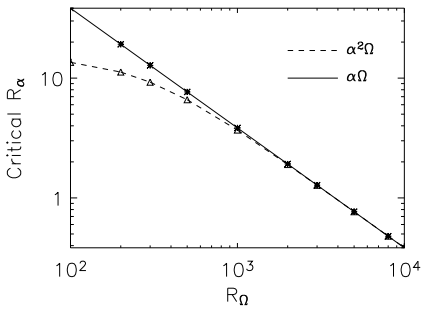

Figure 3. A critical R_α-R_Ω plot for the $\alpha-\Omega$ (solid line) and the $\alpha^2-\Omega$ (dashed line) models for the axisymmetric mode $A0$. When $R_\Omega \leqslant 3\times10^3$, the $\alpha-\Omega$ model has larger critical R_α than the $\alpha^2-\Omega$ one. When $R_\Omega > 3\times10^3$, the two models have the nearly same critical R_α. For the $\alpha-\Omega$ model, $R_\alpha R_\Omega$ is about 3840.

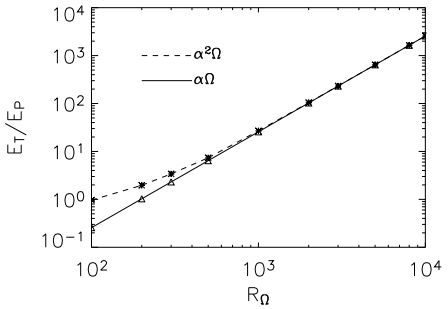

Figure 4. The ratio of the magnetic energy between the toroidal and poloidal components vs. R_Ω for the $\alpha-\Omega$ (solid line) and the $\alpha^2-\Omega$ (dashed line) models for the mode $A0$.

and $\alpha-\Omega$ models and then give the condition for the Sun to excite the preferred non-axisymmetric mode.

3 THE $\alpha^2-\Omega$ DYNAMO MODEL VERSUS THE $\alpha-\Omega$ ONE

For the mean field dynamo theory, poloidal field is created from toroidal field by the α-effect and toroidal field from poloidal field by two ways, i.e. the differential rotation (Ω-effect) and α-effect. The model including all the ingredients is called the $\alpha^2-\Omega$ model. When $R_\Omega \gg R_\alpha^2$, the α-effect as the toroidal source can be ignored. The $\alpha-\Omega$ model is always adopted (Zeldovich et al. 1983). Is the simple $\alpha-\Omega$ model fine for the Sun? What quantitative conditions does it need to satisfy? What are the definite differences between the two models with solar-like parameters?

We first discuss them based on the axisymmetric mode $A0$ and enlarge the range of η_o from 8×10^{10} cm^{2}s^{-1} to 8×10^{12} cm^{2}s^{-1}. Thus we obtain R_Ω ranging from 10^2 to 10^4. For the $\alpha-\Omega$ model, the condition for the generation of undamped magnetic field is only determined by $D=R_\alpha R_\Omega$ (Ivanova & Ruzmaikin 1985). Accordingly we obtain the straight (solid) line in Fig. 3 with logarithmic abscissa and $D=R_\alpha R_\Omega$ is about 3840. But for the $\alpha^2-\Omega$ model, it is more complicated with the generation of toroidal field by the α-effect (the dashed line in Fig.3). Comparing the two lines of Fig. 3, we can see that for the $\alpha^2-\Omega$ model, dynamo action is increased contrasting with the $\alpha-\Omega$ model by the reduction of the critical R_α when R_Ω is small ($<3\times10^3$). With the increasing of R_Ω, the difference for the corresponding critical R_α between the two models decreases. When $R_\Omega=3\times10^3$, the agreement between the two models reaches the level of 0.3%.

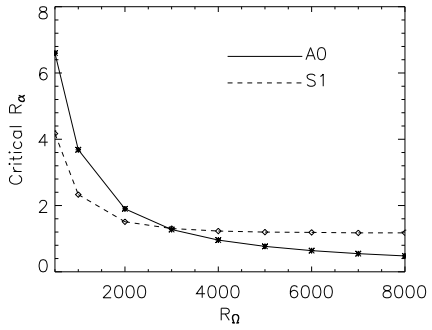

Figure 5. A critical R_α-R_Ω plot for the $\alpha^2-\Omega$ model with the modes $A0$ (solid line) and $S1$ (dashed line). When $R_\Omega \leqslant 3\times10^3$, the mode $S1$ has smaller R_α. It is contrary for $R_\Omega > 3\times10^3$ that the mode $A0$ owns smaller R_α.

Since the absolute scale for the strength of magnetic field is undermined by linear eigenvalues calculations, we define the ratio of the magnetic energy between the toroidal and poloidal components as (Charbonneau & Macgregor 2001):

$$\Theta=\frac{\int B_T^2\ dV}{\int B_P^2\ dV}\ , \tag{22}$$

where $\boldsymbol{B}_T=-\partial g/\partial\theta\ \hat{\mathbf{e}}_\phi$ and $\boldsymbol{B}_P=\frac{L^2h}{r}\ \hat{\mathbf{e}}_r+(\frac{1}{r}\frac{\partial h}{\partial\theta}+\frac{\partial^2h}{\partial r\partial\theta})\ \hat{\mathbf{e}}_\theta$ for the axisymmetric model. Fig. 4 gives the energy ratios between the toroidal and poloidal fields at the onset state for the two models with different R_Ω. When R_Ω is less than 3×10^3, the $\alpha-\Omega$ model produces smaller E_T/E_P than the $\alpha^2-\Omega$ model. The larger R_Ω is, the less difference the two models have. The agreement between the two models reaches 0.46% with $R_\Omega=3\times10^3$. When $R_\Omega>3\times10^3$, the energy ratios are closely in conformity with each other. Thus we can replace the $\alpha^2-\Omega$ model by the $\alpha-\Omega$ model and the corresponding turbulent diffusivity η_o should be less than 2.67×10^{11} cm^{2}s^{-1}.

Let us see the non-axisymmetric mode $S1$ simply now. Table 1 gives the difference for the two models with different R_Ω. When $R_\Omega>4\times10^3$ ($\eta_o<2\times10^{11}$cm^{2}s^{-1}), the difference between the two kinds of models is 0.73% and the two models can be regarded as the same. In a word, if the non-axisymmetric mode $m=1$ is considered in the model, it is necessary for R_Ω to be larger than 4000, namely η_o is less than 2×10^{11}cm^{2}s^{-1} so that the $\alpha-\Omega$ model is at the limit of $\alpha^2-\Omega$ model. It is fully reasonable to adopt the $\alpha-\Omega$ model to replace the $\alpha^2-\Omega$ one.

Table 1. The critical R_α for the $\alpha^2-\Omega$ and the $\alpha-\Omega$ models based on the first non-axisymmetric mode $S1$. $d=(a2-a1)/a2$. $a1$ is the critical R_α for the $\alpha-\Omega$ model and $a2$ for the $\alpha^2-\Omega$ model.

R_Ω	500	1000	2000	3000	4000	5000	6000	7000	8000
$a1$	4.92	2.45	1.545	1.320	1.239	1.203	1.190	1.180	1.179
$a2$	4.17	2.33	1.510	1.306	1.230	1.198	1.186	1.177	1.176
d	18.0	5.15	2.32	1.07	0.73	0.42	0.34	0.25	0.25

4 AXISYMMETRIC VERSUS NON-AXISYMMETRIC MODE

It is commonly regarded that the strong differential rotation works in favor of the axisymmetric mode. Without it, all single main-sequence stars with outer CZs have the non-axisymmetric field configurations (Rüdiger & Elstner 1994). The non-uniform rotation produces the observed dominant oscillatory dipolar field on the Sun. However, is the differential rotation expressed by Eq. (12) is enough to produce the dominant axisymmetric field? What condition does it need to satisfy to make the non-axisymmetric mode preferred?

With the given rotation profile (12) of the Sun, we range R_Ω from 500 to 8000. Accordingly, η_o changes from 1.0×10^{11} cm^{2}s^{-1} to 1.6×10^{12} cm^{2}s^{-1}. Fig. 5 displays the critical R_α with different R_Ω for the $\alpha^2-\Omega$ model. The axisymmetric mode $A0$ (solid line) has lower critical R_α when $R_\Omega>3000$ and will be preferred to excite. It is contrary for $R_\Omega<3000$ that the non-axisymmetric mode $S1$ will have lower critical R_α and will be the preferred mode. The smaller R_Ω is, the easier $S1$ is excited. According to Sec. 3, it is not at the $\alpha-\Omega$ limit ($R_\Omega<3000$) when $S1$ is the preferred mode. In other words, it is impossible to favor the non-axisymmetric mode at the $\alpha-\Omega$ limit. To get the preferred non-axisymmetric modes, the contribution of α-effect to generation of the toroidal field cannot completely vanish (Rädler 1986a). The farther it deviates from the limit, the more important roles the α-effect plays to produce the toroidal field and the easier the non-axisymmetric mode to excite. This is also consistent with the analytical results of Bassom et al. (2005). Furthermore, they gave the reason that the wind-up of non-axisymmetric structures can be compensated by phase mixing inherent to the $\alpha^2-\Omega$ dynamo.

Moreover, rather than the differential rotation, R_Ω is the decisive parameter to decide which kind of mode is preferred. We may also say that the turbulent diffusivity η_o is the key parameter since the differential rotation has been basically determined by the observation (Jiang & Wang 2007). For the $\alpha^2-\Omega$ model, when $R_\Omega<3000$, i.e. $\eta_o>2.67\times10^{11}$ cm^{2}s^{-1} the non-axisymmetric mode will be preferred.

In the coming two sections, we will take the $\alpha^2-\Omega$ model with η_o=1.6×10^{11} cm^{2}s^{-1} and R_Ω=5000 so that the axisymmetric mode will be preferred. This is the real picture of the Sun.

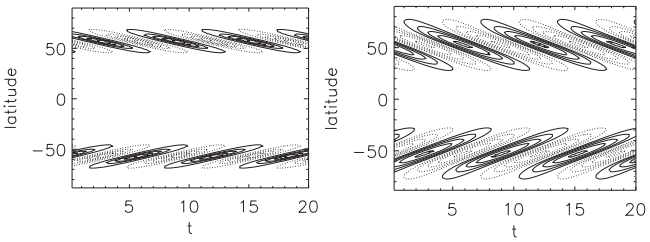

Figure 6. Butterfly diagram of the toroidal field B_ϕ for the mode $A0$ at the depth $r=0.7R_\odot$ (left) and B_r at the surface $r=R_\odot$ (right). Solid (dashed) contours correspond to positive (negative) magnetic field. The diffusion time $R_\odot/\eta_o$ is taken as the time unit.

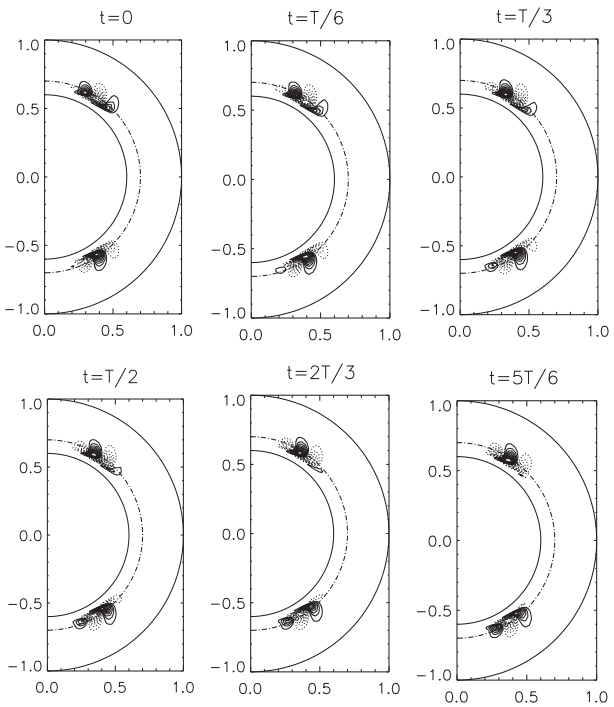

Figure 7. Evolution of the toroidal magnetic field in a meridional plane $\phi=0$ separated by 1/6th of the dynamo period T for the axisymmetric mode $A0$. Solid (dashed) contours correspond to positive (negative) toroidal field. The dot-dashed lines locate at $0.7R_\odot$. The fields concentrate in the tachocline and the high latitudes where the radial shear is strong.

5 THE AXISYMMETRIC MODE

Left part of Table 2 is the truncation levels in the calculation of axisymmetric mode $A0$ and the corresponding critical R_α and frequency ω. N is the radial harmonics expanded in terms of Chebyshev function and L is the harmonics in Legendre function (see Eqs.(16)(17)). When $N=38$ and $L=50$, it gets convergence. The critical R_α is 0.765 and frequency ω is ±410.37. With the dimensionless time $t=R_\odot^2/\eta_o$, we obtain the period is about 15

year, which is a bit shorter than the 22-years solar magnetic cycle. In fact, the meridional circulation omitted in the paper plays an important role in determining the true cycle (Dikpati & Charbonneau 1999). The symbol '$\pm$' corresponds to the dynamo wave propagating equatorward or poleward.

Fig. 6 (left) displays the toroidal field at $r = 0.7R_\odot$ with $\omega = +410.37$. The magnetic field concentrates in the region from latitude 45° to 70° with strong radial shear $\partial\Omega/\partial r < 0$ there. It is well-known that, without meridional circulation, the propagation direction of the dynamo wave is decided by the Parker-Yoshimura sign rule and it should be equatorward since the product of the α-effect and radial gradient of differential rotation is negative (Parker 1955; Yoshimura 1975). The solution with $\omega = -410.37$ corresponds to the dynamo wave propagating poleward. Although some high-frequency dynamo waves were identified to propagate poleward on the Sun (Makarov 1989; Obridko et al. 2006), the poleward solution obtained in our method cannot be used to explain these observations. It is beyond the limitation of our method. Hence, the poleward solution is meaningless and should be neglected. Fig. 6 (right) is a time-latitude diagram of the radial field at the surface. The phase shift between the two components is near $\pi/2$ which is consistent with the observations (Sheeley 1991).

Fig. 7 is the evolution of the toroidal field in a meridional plane $\phi = 0$ at an interval of 1/6th of solar cycle period. The dot-dashed line is $0.7R_\odot$. The magnetic field is among the region where the radial shear of differential rotation is strong, i.e. the high latitude of the tachocline. This follows the general rule that differential rotation tends to destroy any deviation from axisymmetry and toroidal field favors to be produced in the strong radial shear region (Moffatt 1978; Bigazzi & Ruzmaikin 2004).

It seems that the location of the toroidal field produced in the model is higher than that of the observation. Furthermore, when the toroidal flux rope rises through the CZ to emerge, it will have the poleward deflection further due to the effect of Coriolis force (Caligari, Moreno-Insertis, Schüssler 1995). But in the model, we omit an important ingredient, i.e. the meridional circulation. If a meridional circulation is considered, the strong field produced within the tachocline at high latitude will be carried to the low latitudes. The toroidal flux entering the CZ will become buoyantly unstable and emerge to form the active regions at the low latitudes (Nandy & choudhuri 2002).

6 THE NON-AXISYMMETRIC MODE

Right part of Table 2 is the truncation levels of the mode $S1$. When $N = 28$ and $L = 70$, it gets convergence, which is slower than the calculation for the axisymmetric one. The critical R_α is 1.203, much larger than that for the axisymmetric mode. Therefore with taking $R_\Omega = 5000$ and $\eta_o = 1.6 \times 10^{11}\mathrm{cm}^2\mathrm{s}^{-1}$, the axisymmetric mode will be preferred. Fig. 8 is the near surface distribution of the radial magnetic field for the mode $S1$ at the fixed time. The toroidal magnetic field of the mode $m = 1$ superimposed on the axisymmetric toroidal field produces a localized maximum ('hump'). The non-axisymmetric enhancement of the

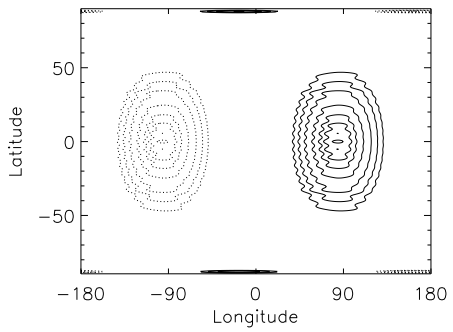

Figure 8. Near surface distribution of the radial component for the mode $S1$ at a fixed time. Solid (dashed) contours correspond to positive (negative) magnetic field.

underlying magnetic field causes the clustering of sunspots to form 'active longitudes' (Ruzmaikin 2001) and 'Flip-flop' which behaves as a special phenomenon of 'active longitudes'.

The frequency ω is -1.022. Hence its period is nearly 400 times longer than that of the mode $A0$. Thus the non-axisymmetric mode $S1$ appears to be rather steady or weakly oscillating comparing to the axisymmetric mode $A0$ (Berdyugina 2004). The time variations of the mode $A0$ are periodical. By changing the sign of the mode $A0$, the predominant longitude jumps by about 180°, which is just the flip-flop phenomenon (see the details of Sec. 3 of Fluri & Berdyugina (2004)). But only based on these two modes, the full flip-flop cycle has the same length as the $A0$ cycle rather than the value which is a 3-4 times shorter (about 3.7 years for the Sun) than the main activity cycle (Berdyugina 2004). There should have more complicated field configuration working on the Sun.

Both the non-axisymmetric and axisymmetric magnetic fields are generated by the same axisymmetric sources. They evolve independently on each other in linear theory. In fact, some nonlinearities, such as non-axisymmetric α-effect (Bigazzi & Ruzmaikin 2004), MHD instability (Dikpati & Gilman 2005), magnetic buoyancy (Chatterjee et al. 2004) and the α-quenching (Zhang et al. 2003; Moss 2005) induce the different modes coupled together and produce the flip-flop cycle (Moss 2004).

Left of Fig. 9 shows the contours of toroidal magnetic field in a meridional plane. All the fields concentrate in the lower part of the tachocline where the diffusivity is less than that of other regions (see Fig. 2). Right of Fig. 9 displays the butterfly diagram for the mode $S1$ at the depth $r = 0.75R_\odot$. The field is mainly concentrated around the 35° latitude, where the radial shear is weak (see Fig. 1). This is consistent with the work of Bigazzi & Ruzmaikin (2004) that the non-axisymmetric field survives only in the weak differential rotation and low diffusivity region.

7 DISCUSSION AND CONCLUSIONS

In this paper we have investigated the properties of the axisymmetric and the non-axisymmetric modes with a linear $\alpha^2 - \Omega$ model in a rotating frame trying to understand

Table 2. Truncation levels and the corresponding critical R_α and frequency ω for the axisymmetric mode $A0$ (left) and the first non-axisymmetric mode $S1$ (right). N and L are the harmonics in Chebyshev function and Legendre function respectively.

N	L	R_α	ω
34	46	0.762	$\pm$408.97
36	46	0.767	$\pm$412.06
38	46	0.764	$\pm$409.90
38	48	0.765	$\pm$410.39
38	50	0.765	$\pm$410.37

N	L	R_α	ω
24	66	1.201	-0.794
26	66	1.198	-0.919
28	66	1.198	-0.967
28	68	1.203	-0.946
28	70	1.203	-1.022

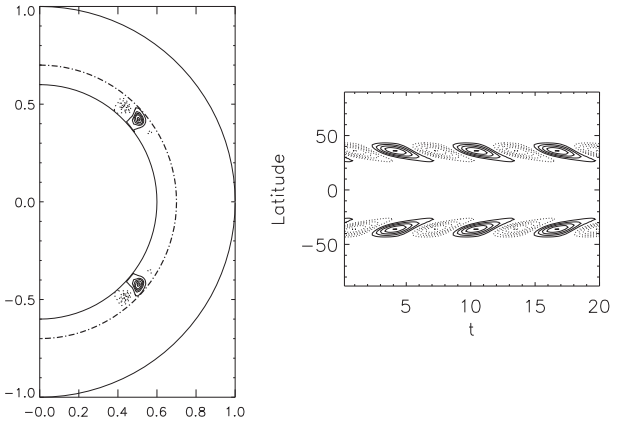

Figure 9. Contours of the toroidal field B_ϕ in a meridional plane (left) and Butterfly diagram of the toroidal field at the depth $r = 0.75R_\odot$ (right) for the mode $S1$. The field concentrates in the low diffusivity (below the dot-dashed line $0.7R_\odot$ in the left diagram) and weak differential rotation (about the latitude 35° in the right diagram) region. Solid (dashed) contours correspond to positive (negative) magnetic field.

the active longitudes, flip-flops and other non-axisymmetric phenomena. The model consists of updated differential rotation, turbulent diffusivity varied with depth and the α-effect working in the tachocline. The definite differences between the $\alpha-\Omega$ and $\alpha^2-\Omega$ models and the conditions to excite the non-axisymmetric modes with the solar-like parameters are presented. The Chebyshev-τ method is used to numerically solve the problem with a high precision. We have tested this code with the analytical solutions of a simple α^2 model and compared with the results of Stix (1976). They matched well with each other.

Although the conditions to favor the non-axisymmetric modes have been investigated by some works (Rädler 1986a,b; Bassom, Kuzanyan, Sokoloff, Soward 2005), we are the first to apply the updated solar parameters with numerical method to obtain these. We also point out the role of the turbulent diffusivity η_o during the process. It is poorly known and cannot be directly deduced from observations. When it is lower than 2.0×10^{11} cm^{2}s^{-1} and R_Ω is larger than 4000 accordingly, the $\alpha-\Omega$ model is at the limit of the $\alpha^2-\Omega$ model. Furthermore, based on the $\alpha^2-\Omega$ model, when R_α is lower than 3000, the non-axisymmetric mode $m = 1$ will be more and more easily excited than the axisymmetric mode $m = 0$ when increasing the value of diffusivity η_o and decreasing the corresponding R_Ω.

The non-axisymmetric mode $S1$ has much longer period than the axisymmetric one $A0$. The co-existence of oscillating mode $A0$ and the nearly steady $S1$ results in the flip-flop phenomenon. Because the differential rotation affects axisymmetric and non-axisymmetric magnetic fields in the different ways, the two kinds of fields prefer to occur in different regions. The axisymmetric magnetic field is mainly concentrated near the high latitude (about 55°) around $0.7R_\odot$, where the radial shear of differential rotation is strong. However, the non-axisymmetric field occurs near the intermediate 35° latitude in the bottom of the tachocline, where the differential rotation is weak and the diffusivity is low.

Usoskin et al. (2005) gave that the ratio between the non-axisymmetric strength and the axisymmetric one is roughly 1:10 by analyzing sunspot group data for the past 120 years. Based on the non-linear models, Moss (1999, 2004) presented the energy ratios between the two kinds of modes although the values cannot match well with the observation. Since our model is linear and different modes are decoupled, it is the limitation to provide the energy ratios between the two modes.

In this work, we regard the strong radial shear only exists in the tachocline and omit the sub-surface shear and other details of the distribution of differential rotation. Brandenburg (2005) argued for the alternative ideas concerning dynamo operating in the bulk of CZ, or perhaps even in the sub-surface shear layer. Moreover, we also only take the α-effect working in the tachocline and ignore the other two possible mechanisms. The two generation sources are still the hot topics on debate. Since we do not aim to give the detailed description of the Sun and just put emphasis on the basic characters of the axisymmetric and non-axisymmetric modes, it is feasible for us to take the two simple generation sources and set up the thin-layer dynamo model. Of course, more rich and realistic models can open new option for the understanding of solar magnetic field.

Furthermore, since we tried to expatiate on our objectives with the simple generation sources, the meridional circulation is not considered in the work. It plays an important role in the axisymmetric mode (Nandy & choudhuri 2002; Guerrero & Muñoz 2004). It carries the strong axisymmetric toroidal field produced at the high latitudes to the low ones and produces the active regions there with the magnetic buoyancy. But it has no much influence on the non-axisymmetric field according to the work of Bigazzi & Ruzmaikin (2004).

In the forthcoming studies we will include the nonlinearities and the meridional circulation to investigate the influence on the coupling of the different modes and the role of meridional circulation in the non-axisymmetric dynamo.

ACKNOWLEDGMENTS

We thank the anonymous referee for valuable comments which have helped in improving the paper. We extend our thanks to A. R. Choudhuri and K. M. Kuzanyan for reviewing the manuscript and giving many helpful comments. JJ would like to thank X. H. Liao and K. K. Zhang for kind supervision on the work. This work has been supported by National Natural Science Foundation of China (10573025, 10603008) and by the National Basic Research Program (G2006CB806303).

REFERENCES

Babcock H. W., 1961, ApJ, 133, 572
Bai T., 1987, ApJ, 314, 795
Bassom A. P., Kuzanyan K. M., Sokoloff D., Soward A. M., 2005, Geophys. Astrophys. Fluid Dynam., 99, 309
Benevolenskaya E. E., Hoeksema J. T., Kosovichev A. G., et al., 1999, ApJ, 517, L163
Berdyugina S. V., Usoskin I. G., 2003, A&A, 405, 1121
Berdyugina S. V., Moss D., Sokoloff D., Usoskin I. G., 2006, A&A, 445, 703
Berdyugina S. V., 2004, Sol. Phy., 224, 123
Bigazzi A., Ruzmaikin A., 2004, ApJ, 604, 944
Brandenburg A., 2005, ApJ, 625, 539
Caligari P., Moreno-Insertis F., Schüssler M., 1995, ApJ, 441, 886
Chan K. H., Liao X., Zhang, K., Jones C. A., 2004, A&A, 423, L37
Chandrasekhar S., 1961, Hydrodynamic and hydromagnetic stability. Oxford: Clarendon Press
Charbonneau P., Christensen-Dalsgaard J., Henning R., Larsen R. M., Schou J., Thompson M. J., Tomczyk S., 1999, ApJ, 527, 445
Charbonneau P., Macgregor K. B., 2001, ApJ, 559, 1094
Chatterjee P., Nandy D., Choudhuri A. R., 2004, A&A, 427, 1019
Choudhuri A. R., 2003, Sol. Phy., 215, 31
De Toma G., White O. R., Harvey K. L., 2000, ApJ, 529, 1101
Dikpati M., Charbonneau P., 1999, ApJ, 518, 508
Dikpati M., Gilman P. A., 2001, ApJ, 551, 536
Dikpati M., Corbard T., Thompson M. J., Gilman P. A., 2002, ApJ, 575, L41
Dikpati M., Gilman P. A., 2005, ApJ, 635, L193
Fluri D. M., Berdyugina S. V., 2004, Sol. Phy., 224, 153
Guerrero G. A., Muñoz J. D., 2004, MNRAS, 360, 317
Ivanova T. S., Ruzmaikin A. A., 1985, Astron. Nachr., 306, 177
Jiang J., Wang J. X., 2006, Chin. J. Astron. Astrophys., 6, 227
Jiang J., Wang J. X., 2007, J. Adv. Space Res., doi:10.1016/j.asr.2007.01.033
Krivodubskii, V. N., 1998, Astronomy Reports, 42, 122
Kuzanyan K. M., Lamburt V. G., Zhang H. Q., Bao S. D., 2003, Chin. J. Astron. Astrophys., 3, 257
Leighton R. B., 1969, ApJ, 156, L1
Obridko V. N., Sokoloff D. D., Kuzanyan K. M., Shelting B. D., Zakharov V. G., 2006, MNRAS, 365, 827
Makarov V. I., 1989, Sol. Phy., 123, 367
Moffatt H. K. 1978, Manetic Field Generation in Electrical Conducting Fluids. Cambridge Univ. Press, Cambridge
Moss D., 1999, MNRAS, 306, 300
Moss D., 2004, MNRAS, 352, L17
Moss D., 2005, A&A, 432, 249
Moss D., Piskunov N., Sokoloff D., 2002, A&A, 396, 885
Nandy D., Choudhuri A. R., 2002, Science, 296, 1671
Neugebauer M., Smith E. J., Feynman J., Feynman J., Vaughan A. H., 2000, J. Geophys. Res., 105, 2315
Parker E. N., 1955, ApJ, 122, 293
Rädler K. H., 1986, ESA SP-251, Plasma Astrophysics, ESA Publications Division, Noordwijk, 569
Rädler K. H., 1986, Astron. Nachr., 307, 89
Rüdiger G., Elstner D., 1994, A&A, 281, 46
Ruzmaikin A., 2001, Space Science Reviews, 95, 43
Schou J., Antia H. M., Basu S. et al., 1998, ApJ, 505, 390
Schubert G., Zhang K. K., 2001, ApJ, 557, 930
Sheeley N. R. Jr, 1991, ApJ, 374, 268
Song W. B., Wang J. X., 2005, ApJ, 624, L137
Stix M., 1971, A&A, 13, 203
Stix M., 1976, A&A, 47, 243
Thelen J.-C., 2000, MNRAS, 315, 165
Usoskin I. G., Berdyugina S. V., Poutanen J., 2005, A&A, 441, 347
Yoshimura H., 1975, ApJ, 201, 740
Zeldovich Ya., Ruzamikin A., Sokoloff D., 1983, Magnetic fields in Astrophysics, Gordon and Breach, New York.
Zhang K., Chan K. H., Zou J., Liao X., Schubert G., 2003, ApJ, 509, 663

APPENDIX A: THE FULL FORM OF THE GOVERNING EQUATIONS

The full forms of the governing equations about the toroidal field g and poloidal field h in (3) and (4) are as follows:

$$\begin{aligned}
\frac{\partial L^2 h}{\partial t} &= R_\alpha[\alpha L^2 g - \frac{\partial \alpha}{\partial \theta}\frac{\partial g}{\partial \theta}] + \eta \nabla^2 L^2 h \\
&- R_\Omega[\Omega \frac{\partial L^2 h}{\partial \phi}] + R_\alpha \frac{1}{\sin\theta}\frac{\partial \alpha}{\partial \theta}[\frac{1}{r}\frac{\partial h}{\partial \phi} + \frac{\partial^2 h}{\partial r \partial \phi}], \quad \text{(A1)} \\
\frac{\partial L^2 g}{\partial t} &= R_\alpha[-\alpha \nabla^2 L^2 h + \frac{\partial \alpha}{\partial \theta}\frac{\partial \nabla^2 h}{\partial \theta} + \frac{\partial^2 \alpha}{\partial r \partial \theta}\frac{\partial^2 h}{\partial r \partial \theta} h \\
&- \frac{\partial \alpha}{\partial r}\frac{\partial L^2 h}{\partial r} - \frac{1}{r}\frac{\partial \alpha}{\partial r} L^2 h - \frac{1}{r^2 \sin\theta}\frac{\partial}{\partial \theta}(\sin\theta \frac{\partial \alpha}{\partial \theta}) L^2 h \\
&- \frac{1}{r^2}\frac{\partial \alpha}{\partial \theta}\frac{\partial L^2 h}{\partial \theta} + \frac{1}{r}\frac{\partial^2 h}{\partial r \partial \theta}] \\
&+ R_\Omega[\frac{1}{r\sin\theta}\frac{\partial}{\partial \theta}[\sin\theta \frac{\partial \Omega}{\partial \theta}\frac{\partial}{\partial r} r(\sin\theta \frac{\partial h}{\partial \theta})] \\
&- \frac{1}{\sin\theta}\frac{\partial}{\partial \theta}[\sin\theta \frac{\partial \Omega}{\partial r}\frac{\partial}{\partial \theta}(\sin\theta \frac{\partial h}{\partial \theta})] \\
&- \frac{1}{\sin\theta}\frac{\partial \Omega}{\partial r}\frac{\partial^2}{\partial \phi^2}\frac{\partial h}{\partial \theta} - \frac{1}{r\sin\theta}\frac{\partial^2}{\partial \phi^2}\frac{\partial}{\partial r}(r\frac{\partial \Omega}{\partial \theta} h)] \\
&+ \eta \nabla^2 L^2 g + \frac{\partial \eta}{\partial r}\frac{\partial}{\partial r} L^2 g + \frac{1}{r}\frac{\partial \eta}{\partial r} L^2 g \\
&+ R_\alpha[\frac{1}{\sin\theta}\frac{\partial g}{\partial \phi}(\frac{\partial^2 \alpha}{\partial r \partial \theta} + \frac{1}{r}\frac{\partial \alpha}{\partial \theta} + \frac{\partial g}{\partial r})] \\
&- R_\Omega L^2(\Omega \frac{\partial g}{\partial \phi}). \quad \text{(A2)}
\end{aligned}$$

where α, Ω and η are the expressions after non-dimensionalization.

This paper has been typeset from a TEX/ LATEX file prepared by the author.